Dalton Transactions

Influence of organic cation planarity on structural templating in hybrid metal-halides

Journal:	*Dalton Transactions*
Manuscript ID	DT-ART-08-2019-003207.R2
Article Type:	Paper
Date Submitted by the Author:	22-Sep-2019
Complete List of Authors:	Oswald, Iain; Colorado State University, Chemistry Ahn, Hyochul; Colorado State University, Chemistry Neilson, James; Colorado State University, Chemistry

SCHOLARONE™
Manuscripts

Influence of organic cation planarity on structural templating in hybrid metal-halides

Iain W. H. Oswald, Hyochul Ahn, and James R. Neilson

Department of Chemistry, Colorado State University, Fort Collins, CO, 80523-1872, United States

E-mail: james.neilson@colostate.edu

Abstract.

Controlling the connectivity and topology of solids is a versatile way to target desired physical properties. This is especially relevant in the realm of hybrid halide semiconductors, where the long-range connectivity of the inorganic substructural unit can lead to significant changes in optoelectronic properties such as photoluminescence, charge transport, and absorption. We present the new series of hybrid metal-halide semiconductors, $(phenH_2)BiI_5 \bullet H_2O$, $(2,2\text{-}bpyH_2)BiI_5$, $(BrbpyH)BiI_4 \bullet H_2O$, $(phenH_2)_2Pb_3I_{10} \bullet 2H_2O$, and $(2,2\text{-}bpyH_2)_2Pb_3I_{10}$ where $(phenH_2)^{2+}$ = 1,10-phenanthroline-1,10-diium, $(2,2\text{-}bpyH_2)^{2+}$ = 2,2'-bipyridine-1,1'-diium and $(BrbpyH)^{+}$ = 6,6′-dibromo-2,2′-bipyridium. These compounds allow us to observe how planarity of the cation, induced either through structural modification in case of $(phenH_2)^{2+}$ or through non-covalent interactions in $(BrbpyH)^{+}$, both relative to $(2,2\text{-}bpyH_2)^{2+}$, modifies the inorganic substructural unit. While the Pb^{2+} series of compounds show minimal changes in inorganic connectivity, we observe large differences in the Bi^{3+} series, ranging from 0-D dimers to corner- and edge-sharing 1-D chains of octahedra. We find that compounds containing $(phenH_2)^{2+}$ and $(BrbpyH)^{+}$ pack more efficiently than those with $(2,2\text{-}bpyH_2)^{2+}$ due to their retention of planarity leading to greater inorganic connectivity. Electronic structure calculations and optical diffuse reflectance reveal that the band gaps of these compounds are influenced by the degree of inorganic connectivity as well as the distances of the inorganic substructural unit distances. These results show that the structure and planarity of organic cations can directly influence both the inorganic connectivity and the optical properties that could be tuned for certain optoelectronic applications.

Introduction

The field of hybrid perovskites and related metal-halide-based semiconductors represents a class of solution processable semiconductors that has undergone a recent renaissance.[1-4] The lattice of these materials is considerably soft when compared to traditional semiconductors (mechanically, as well as hard-soft-acid base), and is relatively modular with respect to incorporation of different metals or organic cations.[5] These materials are typically composed of ammonium containing organic cations and $[MX_6]$

octahedra where M is typically Pb^{2+}, Bi^{3+}, or Sn^{2+} and X is either Cl^-, Br^-, or I^-.[6-9] The connectivity of the inorganic substructural unit is highly dependent on the structure and size of the cation chosen, as well as on the metal used.[10] For instance, the use of smaller organic cations with Pb^{2+} or Sn^{2+} can yield the perovskite structure that has 3-dimensionally connected octahedra such as that observed in $CH_3NH_3PbI_3$ and $CH(NH_2)_2PbI_3$.[5, 11] By using large, primary amine-containing cations such as n-butylammonium or phenethylammonium, layered perovskites can be formed that retain the corner-sharing octahedral motif but in reduced dimensions.[6, 12] Incorporation of cations lacking a primary amine can lead to other structural motifs such as in the case in $(C_7H_7)_2SnI_6$ and $C_7H_7PbI_3$, which have isolated $[SnI_6]^{2-}$ octahedra and face-sharing chains of $[PbI_6]^{4-}$ octahedra, respectively. Using Bi^{3+} as the metal often results in structures where face- and edge-sharing octahedral structural subunits are observed.[13-14] This is the case in the compounds $Cs_3Bi_2I_9$ and $(C_7H_7)BiI_4$: the former are composed of face-sharing dimers of $[BiI_6]$ octahedra, while the latter has edge-sharing chains of octahedra.[15-16] In each of these, the structure of the compounds directly affects the optoelectronic properties: For instance, greater inorganic connectivity typically results in smaller band gaps, a property that has been exploited when targeting desired functionalities.

Although these examples exist showing the different types of connectivity possible in this family of materials, the question remains, how do organic cations template the overall structure in hybrid metal halides and how do the optoelectronic properties change with templating?[10] This is especially true for compounds that have non-primary amines or that are sterically encumbered, as there are fewer reported compounds of this type. Additionally, the HOMO/LUMO states of the organic cations are typically well above the conduction band or well below the valence band, essentially removing their participation in electronic or optical properties. By using fully aromatic containing cations, one can obtain new structures altogether, where the organic cation structure can direct the connectivity of the inorganic substructural unit while contributing to the frontier electronic states of the material. This has recently been shown in the compounds $(C_7H_7)MX_4$ (M = Bi^{3+}, Sb^{3+}; X = Cl^-, Br^-, I^-)[16] and $(C_7H_7)_2SnI_6$ and $C_7H_7PbI_3$,[17] where the valence band is derived from the halide p-orbitals and the conduction band the π*-states on the tropylium ($C_7H_7^+$) cation. Another example of using a highly-aromatic optoelectronically-active cation in hybrid metal halides is the compound (Pb_2I_6)•(H_2DPNDI)•(H_2O)•(NMP), where DPNDI = N,N'-di(4-pyridyl)-1,4,5,8-napthalenediimide and NMP: N-methylpyrrolidin-2-one.[18] Here, the cations direct the inorganic substructural unit $[Pb_2I_6]$ to form 1-D chains with the H_2DPNDI molecules packing such that the π-cloud of the aromatic moiety interacts with the inorganic chains. This leads to efficient spatial charge separation in the excited state, with holes residing on the inorganic unit and electrons on the organic unit. Another recent study showed that (*N*,*N*′-dialkyl-4,4′-bipyridinium) and other related (*N*,*N*'-R_1,R_2-4,4-bipyridinium) cations can be used to template pseudo-1D $[Pb_2I_6]$ chains, where the choice of *R*-group can help enhance

the π- π stacking between neighboring cations and reduce the band gap of the material. Although these examples exist showing that the organic cation structure can influence the inorganic substructure, it is difficult to predict how this will occur.

In addition to the question of how the structure of the organic cation can direct the inorganic connectivity in the crystal structure, few studies exist that investigate how halogenation of organic cations affects structure in hybrid metal halides,[19-21] especially with heavier halogens such as bromine or iodine.[22-25] One example of heavy halogen containing cations is in the Ruddlesden-Popper compounds $(A)_2[PbI_4]$ (A = BYA (but-3-yn-1-ammonium), BEA (but-3-en-1-ammonium), PEA (prop-2-en-1-ammonium), and BYA-I2 ((E)-3,4-diiodobut-3-en-1-ammonium)), which can undergo addition of iodine across the unsaturated bond upon exposure to I_2 vapor.[23] In some cases, the iodine could be reversibly removed to yield the initial non-iodinated compounds. The authors report drastic changes in physical color as well as lattice parameter, indicating changes in both the crystal structure and the optoelectronic properties. Another study looked at the compounds $[(BrC_2H_4NH_3)_2PbI_4]$ and $[(IC_nH_{2n}NH_3)_2PbI_4]$ (n = 2–6), which have Br or I located at the terminal carbon atom of the cation.[22] It was noted that the large halogens affect the packing of the 2-D perovskites, with the tilt angle having to adjust for the larger atoms in the interlayer gallery. These examples show that incorporating heavy atoms can have a direct effect on structure and optoelectronic properties; however, no examples exist looking at fully conjugated cations nor investigate compounds that have non-covalent interactions between the heavy atoms on the cation and the inorganic substructural unit.

Here we report how planarity of organic cations, through either structural modification or non-covalent interactions, modifies the connectivity of the inorganic substructural unit in a new series of compounds. We explore how the dicationic forms of 2,2'-bipyridine (2,2'-bipyridine-1,1'-diium = 2,2-bpyH_2) and 1,10-phenanthroline (1,10-phenanthroline-1,10-diium = phenH_2), which can be considered structurally unconstrained and planar, respectively, modify the structure and resulting optoelectronic properties of the compounds $(2,2\text{-bpyH}_2)_2Pb_3I_{10}$, $(phenH_2)_2Pb_2I_{10}\bullet 2H_2O$, $(2,2\text{-bpyH}_2)BiI_5$, and $(phenH_2)BiI_5\bullet H_2O$. We then see how bromination of 2,2'-bipyridine influences the structure by incorporating 6,6'-dibromo-2,2'-bipyridine (6,6'-dibromo-2,2'-bipyridinium = BrbpyH) to yield the compound $(BrbpyH)BiI_4\bullet H_2O$,as this cation can induce non-covalent halide-halide interactions with the inorganic unit, allowing us to probe an indirect method of making the cation more planar. We find that the connectivity within the Pb^{2+} series is not changed drastically, with each having 1-D chains of differing connectivity. On the other hand, the $[BiI_6]$ octahedra in the Bi^{3+} series have significantly different connectivity, ranging from dimers in $(2,2\text{-bpyH}_2)BiI_5$, corner sharing chains in $(phenH_2)BiI_5\bullet H_2O$, to face-sharing chains in $(BrbpyH)BiI_4\bullet H_2O$. These changes in connectivity relate to how efficiently the organic

cations pack, with $(phenH_2)^{2+}$ and $(BrbpyH)^{+}$ having greater π-stacking leading to greater long-range connectivity. We also find that along with the degree of inorganic connectivity, one of the other predominant factors contributing to the band gap energy is the inter-inorganic substructural unit distance (i.e., the closest iodine-iodine contacts between unconnected $[BiI_6]^{3-}$ moieties), with compounds with smaller distances having smaller gaps. These results show that planarity, size, and halogenation of the cations can be used to direct the structure of the inorganic substructural units that can be exploited when targeting compounds with specific functionality.

Experimental.

Synthesis.

$(phenH_2)BiI_5 \cdot H_2O$. A 0.200 M Bi^{3+} stock solution in stabilized HI (57 wt-% in H_2O, <1.5% H_3PO_2) was first made by dissolving 0.261 g (1.00 mmol) of BiOCl into 5 mL of HI under magnetic stirring, resulting in a clear, dark red solution. After complete dissolution, phenanthroline monohydrate (0.396 g, 2.00 mmol) was dissolved into 1 mL of HI (aq, <1.5% H_3PO_2) and then transferred to the Bi^{3+} stock solution resulting in precipitation of a dark red microcrystalline powder. The solid was then filtered and washed with acetic acid and hexanes. Yield: 0.814 g (0.780 mmol); 78% based on Bi^{3+} content.

$(phenH_2)_2Pb_3I_{10} \cdot 2H_2O$. A 0.200 M Pb^{2+} stock solution in stabilized HI (57 wt-% in H_2O, <1.5% H_3PO_2) was first made by dissolving 0.223 g (1.00 mmol) of PbO into 5 mL of HI under magnetic stirring, resulting in a clear, bright yellow solution. After complete dissolution, phenanthroline monohydrate (0.396 g, 2.00 mmol) was dissolved into 1 mL of HI (aq, <1.5% H_3PO_2) and then transferred to the Pb^{2+} stock solution resulting in precipitation of a dark red microcrystalline powder. The solid was then filtered and washed with acetic acid and hexanes. Yield: 0.542 g (0.237 mmol); 71% based on Pb^{2+} content.

$(2,2\text{-}bpyH_2)_2Pb_3I_{10}$. A 0.200 M Pb^{2+} stock solution in stabilized HI (57 wt-% in H_2O, <1.5% H_3PO_2) was first made by dissolving 0.223 g (1.00 mmol) of PbO into 5 mL of HI under magnetic stirring, resulting in a clear, bright yellow solution. After complete dissolution, 2,2-bipyridine (0.312 g, 2.00 mmol) was dissolved into 1 mL of HI (aq, <1.5% H_3PO_2) and then transferred to the Pb^{2+} stock solution resulting in precipitation of a red microcrystalline powder. The solid was then filtered and washed with acetic acid and hexanes. Yield: 0.470 g (0.213 mmol); 64% based on Pb^{2+} content.

$(2,2\text{-}bpyH_2)BiI_5$. A 0.200 M Bi^{3+} stock solution in stabilized HI (57 wt-% in H_2O, <1.5% H_3PO_2) was first made by dissolving 0.261 g (1.00 mmol) of BiOCl into 5 mL of HI under magnetic stirring, resulting in a clear, dark red solution. After complete dissolution, 2,2-bipyridine (0.312 g, 2.00 mmol) was dissolved into 1 mL of concentrated HI and then transferred to the Bi^{3+} stock solution resulting in precipitation of a

bright orange microcrystalline powder. The solid was then filtered and washed with acetic acid and hexanes. Yield: 0.671 g (0.670 mmol); 67% based on Bi^{3+} content.

(BrbpyH)BiI_4•H_2O. A 0.200 M Bi^{3+} stock solution in HI (57 wt-% in H_2O, <1.5% H_3PO_2) was first made by dissolving 0.521 g (2.00 mmol) of BiOCl into 10 mL of concentrated HI under magnetic stirring, resulting in a clear red/orange solution. After complete dissolution, 6,6'-dibromo-2,2'-bipyridine (0.191 g, 0.600 mmol) was directly dissolved into 3 mL of 0.200 M Bi^{3+} stock solution (0.600 mmol) with a ratio of Brbpy:Bi = 1:1, resulting in precipitation of a bright, orange crystalline powder. The solution stirred for 15 minutes, and the solid was filtered and washed with acetic acid and diethyl ether. Yield: 0.516 g (0.492 mmol); 82% based on Bi^{3+} content.

Powder X-ray Diffraction. Laboratory powder X-ray diffraction data were collected on a Bruker D8 Discover DaVinci Powder X-ray Diffractometer using Cu Kα radiation and a Lynxeye XE-T position-sensitive detector. Samples were prepared on a zero-diffraction Si wafer by sprinkling the microcrystalline powder directly onto the substrate. TOPAS6 was used for Rietveld refinements of the data. These data are shown in Supporting information.

Single Crystal X-ray Diffraction. Laboratory Singe Crystal X-ray diffraction data was collected at room temperature using a Bruker D8 Quest ECO diffractometer equipped with a microfocus Mo Kα radiation source and Photon 50 CMOS half-plate detector. Single crystals were mounted onto a MiTeGen tip using paratone oil. Bruker SAINT was used for integration and scaling of collected data and SADABS was used for absorption correction.[26] Starting models for the compounds were generated using the intrinsic phasing method in SHELXT.[27] SHELXL2014 was used for least-squares refinement.[28] The PLATON suite was used to determine higher symmetry and for structural validation.[29] Hydrogen atoms on water molecules were located by investigating the residual electron density surrounding the oxygen atoms and assigning them based on chemically reasonable positions. They were constrained using the DFIX command to ensure reasonable bond lengths. Refinement of the H1 atom occupancy in (BrbpyH)BiI_4•H_2O revealed approximately 50% occupancy (0.55(11)). Therefore, the occupancy was locked at 50%, which results in charge balancing of the overall compound. Structural details of the refinement and crystallographic parameters are listed in in Table 1.

DFT calculations. Density functional theory calculations within the plane-wave code VASP (*Vienna Ab initio Simulation Package*) were performed.[30-31] To treat the effects of exchange and correlation, the PBEsol functional, a version of the Perdew, Burke and Erzorhof (PBE) functional revised for solids was used.[32-33] Valence-core interactions were described with the projector augmented wave method. The experimental crystals structures of all compounds were relaxed in the Niggli-reduced cell by allowing all ions to move

and allowing the unit cell shape and size to vary; convergence was achieved when forces on all the ions were less than 0.001 eV $Å^{-1}$. Relaxations of the ionic positions were conducted using k-point meshes generated using the Monhorst-Pack scheme in steps smaller than 0.02 $Å^{-1}$ and using an energy cutoff of 530 eV.

Densities of states (DOS) and band structures were calculated with explicit inclusion of spin orbit coupling (SOC). DOS were calculated using k-point meshes in steps of ~0.015 $Å^{-1}$; the band structure was calculated across high symmetry points as defined by Setyawan and Curtarolo.[34] DOS and band structures were visualized using the sumo package.[35] Band-decomposed charge densities were computed from the highest occupied and lowest unoccupied bands and visualized using VESTA.[36] In the case of (BrbpyH)BiI_4•H_2O, which has a 50% occupied H atom on both nitrogen atoms of the Brbpy moiety, we constructed a supercell in *P*1 and then manually removed every other hydrogen atom in order to ensure each molecule was singly protonated to retain charge neutrality of the overall compound.

Optical Diffuse Reflectance Spectroscopy. UV-visible diffuse reflectance spectroscopy was performed on powdered samples of each compound diluted to ~10 wt % with $BaSO_4$, using $BaSO_4$ as a baseline. Spectra were acquired using a Thermo Nicolet Evolution 300 spectrophotometer with a Praying Mantis mirror setup from λ = 200 to 1100 nm at a scan rate of 240 nm/min.

Results and Discussion.

The compounds reported represent new entries in the growing phase space of hybrid metal halides, with each having their own unique crystal structure as determined by single crystal X-ray diffraction. The crystallographic data for each compound can be found in Table 1. The organic molecules 1,10-phenanthroline (phen) and 2,2'-bipyridine (2,2-bpy) become doubly protonated and therefore function as dications that are fully conjugated, juxtaposed to the more commonly used aliphatic primary ammonium containing di-cations such as 1,4-diammonium.[37] Curiously, 6,6'-dibromo-2,2'-bipyridine (Brbpy) only becomes singly protonated in (BrbpyH)BiI_4•H_2O. We note that attempts at growing crystals of the Pb^{2+} analogue using Brbpy were successful; however, the crystal quality was not high enough to ensure accurate and reliable structural determination. Phenanthroline represents the "rigid" and planar analogue to 2,2-bpy as the C–C backbone bridging the two pyridine rings prevents free rotation around the 2-positioned carbon atoms, while Brbpy gives a handle for inducing planarity indirectly via cooperative halide-halide interactions with the inorganic substructural unit. Figure 1 shows the molecular structures of 2,2-bpy, phen, and Brbpy and the corresponding inorganic substructural unit obtained when reacted with either Pb^{2+} or Bi^{3+} in HI (aq).

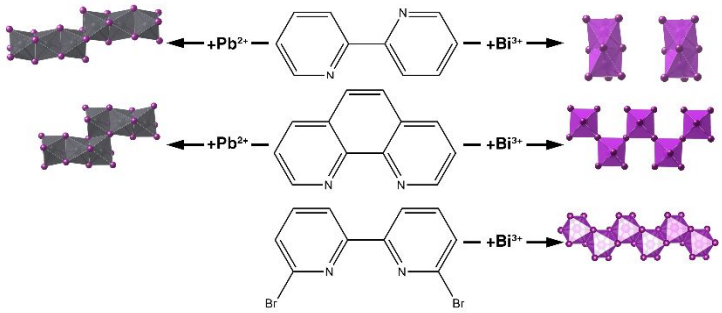

Figure 1. Schematic showing the different inorganic substructural units obtained upon reaction with 2,2-bpy, phen, or Brbpy with the respective metals in hydroiodic acid (*aq*).

Table 1. Experimental Crystallographic Parameters From Single Crystal Diffraction

Compound	$(2,2\text{-bpyH}_2)_2Pb_3I_{10}$	$(phenH_2)_2Pb_3I_{10}\bullet 2H_2O$	$(2,2\text{-bpyH}_2)BiI_5$	$(phenH_2)BiI_5\bullet H_2O$	$(BrbpyH)BiI_4\bullet H_2O$
Crystal System	Monoclinic	Monoclinic	Triclinic	Monoclinic	Monoclinic
Space Group	*C*2/*c*	$P2_1/n$	$P\bar{1}$	*P*2/*c*	*C*2/*c*
a (Å)	23.0581(9)	8.5780(5)	9.9732(4)	8.8873(16)	16.8894(12)
b (Å)	9.6584(4)	14.1272(9)	10.5908(5)	12.724(2)	16.2437(11)
c (Å)	20.2649(8)	18.0628(12)	19.3664(9)	19.021(3)	7.7193(5)
α (°)	90	90	80.227(2)	90	90
β (°)	115.4910(10)	93.434(2)	88.320(2)	98.769(5)	108.266(2)
ɣ (°)	90	90	88.114(2)	90	90
V (Å^3)	4073.7(3)	2185.0(2)	2014.20(16)	2125.7(6)	2011.1(2)
Z	4	2	2	4	4
Crystal dimensions (mm^3)	0.07 x 0.06 x 0.02	0.11 x 0.08 x 0.02	0.09 x 0.02 x 0.01	0.13 x 0.05 x 0.03	0.11 x 0.06 x 0.01
θ range (°)	2.32 – 26.48	2.68 – 26.45	2.28 – 26.47	2.69 – 26.39	2.5 – 26.5
μ (mm^{-1})	19.96	18.62	16.41	15.56	18.88
Temperature (K)	300	300	300	300	300
Measured Reflections	27016	12858	64662	14836	10201
Independent Reflections	4203	4458	8392	4349	2095
Reflections with $I > 2\sigma(I)$	3436	3762	6482	3487	1887
R_{int}	0.042	0.041	0.065	0.055	0.035
$R_1(F)^a$	0.028	0.030	0.040	0.041	0.025
$wR_2{}^b$	0.070	0.074	0.097	0.105	0.060
Parameters	168	205	199	197	98
Goodness-of-fit on F^2	1.07	1.05	1.04	1.04	1.07

$^aR_1 = \Sigma||F_o| - |F_c||/ \Sigma|F_o|$. $^bwR_2 = [\Sigma[w(F_o^2 - F_c^2)^2]/ \Sigma[w(F_o^2)^2]]^{1/2}$.

Structural analysis of $(2,2\text{-bpyH}_2)BiI_5$ and $(2,2\text{-bpyH}_2)_2Pb_3I_{10}$

The structural isomerism of 2,2-bpy is the first consideration in these structures. The *trans* configuration of 2,2-bpy has a lower energy compared to the *cis* configuration and is therefore more probable to exist in these compounds.[38-39] This can be explained by the electrostatic repulsion experienced by the protonation of both nitrogen positions in strong acidic media to favor the trans configuration, or the repulsion of N-based lone pairs in the neutral molecule. The *trans* configuration of 2,2-bpy is observed in both $(2,2\text{-bpyH}_2)BiI_5$ and $(2,2\text{-bpyH}_2)_2Pb_3I_{10}$.

The structure of $(2,2\text{-bpyH}_2)_2Pb_3I_{10}$ is composed of $[PbI_6]$ pseudo-1-D chains that have a combination of edge- and face-sharing octahedra (Figure 2) separated in space by 2,2-bpy molecules. Unlike other previously reported compounds with large organic cations that have significant overlap between neighboring cations such as $(C_7H_7)MX_4$ (M = Bi^{3+}, Sb^{3+}; X = Cl^-, Br^- and I^-),[16] the 2,2-bpy molecules pack to have negligible π-orbital overlap between them. This could partially be due to the fact that the 2,2-bpy molecules are not completely planar, whereas in $(C_7H_7)MX_4$ (M = Bi^{3+}, Sb^{3+}; X = Cl^-, Br^- and I^-), the tropylium cations ($C_7H_7^+$) retain their planarity, which would favor π-stacking.

The unit cell in $(2,2\text{-bpyH}_2)_2Pb_3I_{10}$ has one unique $2,2\text{-bpy}^{2+}$ molecule that contains two independent nitrogen positions, N1 and N2. To determine the correct positions of these on the pyridine rings during single crystal X-ray diffraction refinements, we first switched the location of N1 and C4, which would lead to a hypothetical *cis* configured geometry. The occupancies refine to be over- and under-occupied for both, respectively, with values of ~1.28 and 0.79 each. When the N1 and C4 are refined in their correct positions, their occupancies are ~1, the expected value for a correctly assigned atom. We then conducted the same test for the other pyridine ring by switching the N2 and C7 positioned atoms with one another. Again, this led to similarly erroneous occupancies, suggesting their positions are indeed correct as reported and confirming the *trans* configuration.

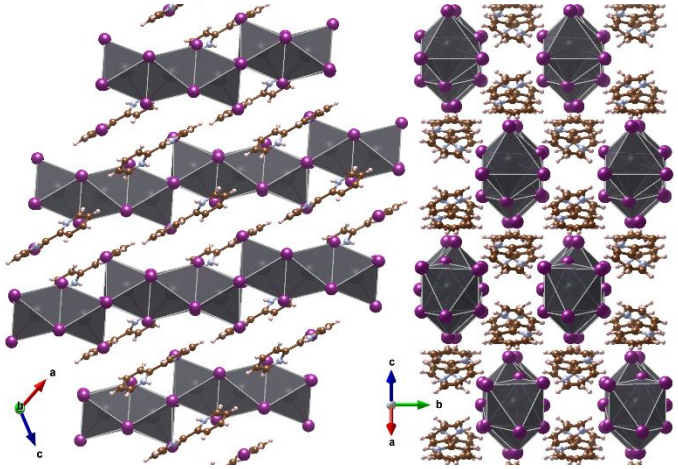

Figure 2. Crystal structured viewed along different directions of $(2,2\text{-bpyH}_2)_2Pb_3I_{10}$. The $2,2\text{-bpyH}_2$ molecules act to separate the 1-D $[PbI_6]$ chains from one another.

We conducted similar tests on $(2,2\text{-bpyH}_2)BiI_5$ by switching the locations of the N and C atoms on the pyridine rings to ensure their positions were accurate. This structure has three unique $2,2\text{-bpy}^{2+}$ molecules versus just one in $(2,2\text{-bpyH}_2)_2Pb_3I_{10}$ due to the overall lower symmetry of the structure ($P\bar{1}$). Two of the molecules have their rings pointed towards an isolated iodine atom in the structure (Figure 3, right), while the third is located near the inorganic $[Bi_2I_9]$ dimer; this unit is similar to that observed in

$Cs_3Bi_2I_9$, composed of two face-sharing [BiI_6] octahedra.[15] For the former, each molecule has its second pyridine ring generated through symmetry, which leads to only one unique nitrogen position per molecule in a *trans* configuration. This is shown in Figure 3 where the unique N1 and N2 atoms and their symmetry generated N1' and N2' atoms are shown in blue, and the unique carbon atoms C4 and C9 and their respective atoms C4' and C9' are shown in red. We allowed the occupancies of the N2, C9, N1 and C4 positions to freely refine, resulting in values near ~1 for each. When we switched the locations on each ring (N2 for C9 and N1 for C4), the occupancies became over and under occupied, confirming that the initial positions of atoms are indeed correct. We also note that this *trans* configuration is further supported by the fact that the shortest X•••I^- bonds (X = N or C) are N1•••I^- and N2•••I^- as shown in Figure 3. The more polar N–H versus C–H bond would favor a stronger electrostatic interaction with the neighboring free iodine atom leading to the shorter bond lengths. The third 2,2-bpy molecule, which is located closer to the [Bi_2I_9] dimer, is composed entirely of unique positions. We again tested the different possible configurations of N and C atoms on the rings by monitoring their occupancies as a function of atom, either N or C; these tests again confirmed the trans configuration for this molecule to be correct.

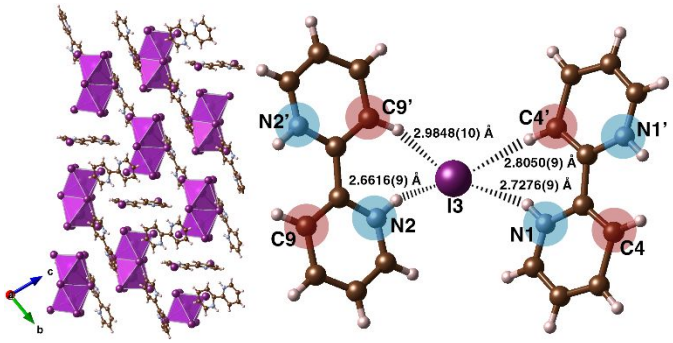

Figure 3. Left: Crystal structure of (2,2-bpyH_2)BiI_5 showing the inorganic [Bi_2I_9]$^{3-}$ dimers separated in space by the 2,2-bpy molecules, reminiscent of $Cs_3Bi_2I_9$ and $(CH_3NH_3)_3Bi_2I_9$. Right: Local environment of two 2,2-bpy molecules coordinating to I^-, their symmetry generated positions, and bond lengths.

Structural analysis of $(phenH_2)_2Pb_3I_{10}$•$2H_2O$ and $(phenH_2)BiI_5$•H_2O

Unlike 2,2-bpy, phen does not isomerize and therefore has nitrogen atoms in proximal locations, akin to a *cis* configuration of 2,2-bpy. The C–C backbone also prevents the molecule from undergoing any torsional twisting, ensuring the molecule remains planar. We find that this also has another consequence: In both structures, water is hydrogen bonded to the N–H bonds of the phen molecules, which is then in close proximity to the inorganic subunit where it presumably has a modest interaction with the iodine atoms to stabilize the compounds.

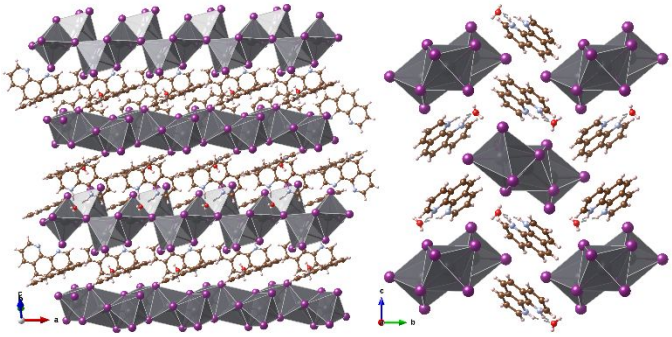

Figure 4. Left: Crystal structure of $(phenH_2)_2Pb_3I_{10}•2H_2O$ showing the inorganic $[PbI_6]$ chains separated in space by the phen molecules. Right: packing arrangement of 2,2-bpy molecules surrounding the inorganic chains.

The structure of $(phenH_2)_2Pb_3I_{10}•2H_2O$ is composed of 1-D chains of $[PbI_6]$ octahedra with both edge and face sharing connectivity, similar to $(2,2\text{-}bpyH_2)_2Pb_3I_{10}$. These octahedra are then separated in space by phen molecules with the hydrogen bonded water residing near the *cis* configured N–H bonds (Figure 4, left). The phen molecules pack around the inorganic chains to form off-set π-stacked chains themselves (Figure 4, right). The inorganic chains are composed of edge and face-sharing octahedra, however differ from $(2,2\text{-}bpyH_2)_2Pb_3I_{10}$ in their connectivity. In $(phenH_2)_2Pb_3I_{10}•2H_2O$, there exist face-sharing trimers of $[Pb_3I_{12}]$ that are connected to one another on their edges that are roughly parallel to the chain. This creates an offset-type chain grown pattern, while $(2,2\text{-}bpyH_2)_2Pb_3I_{10}$ shares edges perpendicular to the direction of the chain, allowing the chains to grow in a straight-line pattern.

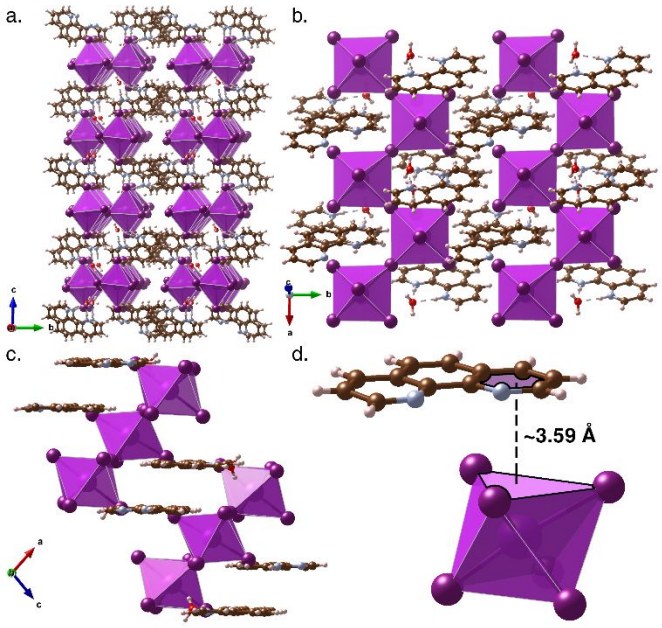

Figure 5. a. Crystal structure of $(phenH_2)BiI_5•H_2O$ showing the corner-sharing $[BiI_6]$ octahedral chains separated in space by the phen molecules. b. Top-down view showing the closed-packing of two

neighboring inorganic chains. c. Crystal structure showing planar packing of phen molecules separating [BiI_6] chains d. Haptic-like interaction between the pyridyl ring of the phen molecule and a face of a neighboring [BiI_6] octahedra.

(phenH_2)BiI_5•H_2O is one of the few Bi^{3+} compounds that has perovskite-like corner-sharing octahedra (Figure 5). This compound has phen coordinating to water like (phenH_2)$_2Pb_3I_{10}$•$2H_2O$, with the H_2O molecule roughly located in between the zig-zagging (110)-perovskite inorganic octahedral chains (Figure 5, right). As the phen group is quite bulky, it prevents the [BiI_6] octahedral layers from forming layers, such as that seen in 2-D perovskites such as $(CH_3(CH_2)_3NH_2)_2PbI_4$ or $((CH_3)_2CHCH_2NH_3)PbI_4$.[40] The inorganic chains propagate along the *a*-axis of the unit cell, with neighboring chains having relatively close contacts of 3.9363(14) Å, similar to that observed for other compounds that have unconnected yet closed packed type inorganic substructures.[16] The phen molecules pack roughly planar to one another, with a haptic-like interaction occurring between one of the pyridyl rings and a face of the inorganic octahedra. This type of interaction could facilitate charge transfer between the organic and inorganic units, possibly leading to efficient spatial charge separation.

Structural analysis of (BrbpyH)BiI_4•H_2O

The final structure to describe is (BrbpyH)BiI_4•H_2O. Although $BrbpyH^+$ can potentially rotate around the 2-positioned carbon to yield a trans configuration, we find it adopts a *cis* configuration in both compounds. This is somewhat unexpected based solely on the argument of steric effects and electrostatic repulsion, as one might expect the bromine and nitrogen atoms on each pyridine ring to spatially separate from one another as far as possible, which would yield a *trans* configuration. However, we suspect that the primary reason for this not occurring is due to two things: First, unlike the cations in the previously described compounds, Brbpy is only singly protonated in (BrbpyH)BiI_4•H_2O. This is evident by refinement of the occupancy of the H1 atom in (phen)BiI_4•H_2O: H1 is located on the nitrogen atoms of both pyridine rings of the cation due to symmetry (occupancy refines to 0.55(11)). Given the large degree of potential dynamical disorder in this material and low scattering contrast of light elements, this occupancy was set to 50% between each position next to a nitrogen atom. This indicates that the hydrogen is only on one of the nitrogen atoms at a time, while helping satisfy the formal charge of the compound, whereas a doubly protonated $(BrbpyH_2)^{2+}$ would make the overall charge +1. Having only one nitrogen protonated may instead favor the *cis* configuration as there are less steric effects between the two nitrogen atoms than when doubly protonated; however, we cannot rule out that this isomer is instead favored due to the nature of molecular packing in the lattice.

The BrbpyH molecules can adopt a *cis* configuration to maximize non-covalent interactions with the inorganic sublattice. In both compounds, the bromine atoms appear to pack such that they interact

strongly with the neighboring inorganic substructural unit via short Br–I distances. In (BrbpyH)BiI_4•H_2O, neighboring $(BrbpyH)^+$ cations pack roughly 180° from one another in columns that act to separate the inorganic unit (Figure 6, left). The bromine atoms face the nearest [BiI_6] octahedra to yield relatively short Br–I contacts of 3.9635(10) Å. This also allows the Brbpy to pack such that they have near total planarity (Figure 6, right), enhancing the interactions between the neighboring molecules. This packing allows the inorganic unit to form extended edge-sharing chains, which is similar $(C_7H_7)MX_4$ ($M = Bi^{3+}$, Sb^{3+}; $X = Cl^-$, Br^-, I^-) and is the same octahedral connectivity found in BiI_3.[16]

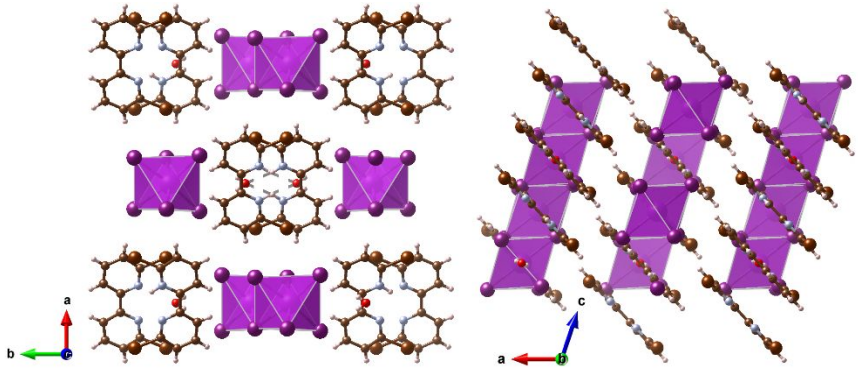

Figure 6. Left: Crystal structure of (BrbpyH)BiI_4•H_2O viewed down the direction of the Brbpy columns and [BiI_6] chains. Right: Packing arrangement of $(BrbpyH)^+$ showing near total planarity of molecules.

The impact of organic cation planarity and halogenation on structure and properties

The inclusion of phen, 2,2-bpy, or Brbpy molecules during the synthesis reactions allows us to compare how planarity impacts the structure and resulting properties. As phen is more planar and sterically bulkier than 2,2-bpy, comparisons can be made between how this contrast influences the optoelectronic properties, as represented by (phenH_2)BiI_5•H_2O vs. (2,2-bpyH_2)BiI_5. (phenH_2)BiI_5•H_2O exhibits corner-sharing [BiI_6] octahedra separated by the phen molecules to form 1-D chains, while (2,2-bpyH_2)BiI_5 has only dimeric inorganic units composed of face-sharing [BiI_6] units. The latter forms most likely due the strong preference for a *trans* configuration of 2,2-bpy, especially once doubly protonated. The ability to twist torsionally around the C–C bond linking the two pyridine rings also prevents efficient π-stacking such as that seen in the planar phen cases, which then prevents extended connectivity of the inorganic octahedra.

On the other hand, $(BrbpyH)^+$ represents an intermediate case between $(phenH_2)^{2+}$ and $(2,2\text{-}bpyH_2)^{2+}$: $(BrbpyH_2)^{2+}$ can rotate around the C–C bond like $(2,2\text{-}bpyH_2)^{2+}$ but has more steric hinderance due to the large bromine atoms at the 6-positions. Nonetheless, we find $(BrbpyH)^+$ adopts a *cis* configuration in (BrbpyH)BiI_4•H_2O yielding a structure with efficient packing of the organic molecules into columns.

This packing motif most likely occurs due to the propensity to form non-covalent Br•••I interactions between the $(BrbpyH)^+$ cations that interact with the neighboring $[BiI_{4/2}I_{2/1}]^-$ chains. These results suggest that the cooperative interactions between the organic halogen atoms and the inorganic halogens can effectively increase the planarity of the cation allowing it retain planarity, similar to that seen in $(phenH_2)BiI_5•H_2O$. Therefore, it appears that having greater planarity, whether through non-covalent interactions between the organic and inorganic substructural units or via functionalization of the organic to eliminate torsional twisting leads to more efficient packing of the organic cations, and thus the ability to template the inorganic octahedra into extended structures.

The difference in structures between $(phenH_2)_2Pb_3I_{10}•2H_2O$ and $(2,2\text{-}bpyH_2)_2Pb_3I_{10}$ is more subtle than the Bi^{3+} compounds. We again observe *trans* configured 2,2-bpy in $(2,2\text{-}bpyH_2)_2Pb_3I_{10}$, where in $(phenH_2)_2Pb_3I_{10}•2H_2O$ the nitrogen atoms are in the *cis* configuration. Each contain chains of $[PbI_6]$ octahedra but with different connectivity in each. $(phenH_2)_2Pb_3I_{10}•2H_2O$ and $(2,2\text{-}bpyH_2)_2Pb_3I_{10}$ both have face and edge-sharing octahedra. The packing of the organic molecules in each compound is similar: The cations orient around the inorganic chains to form columns, although there is greater π-stacking in $(phenH_2)_2Pb_3I_{10}•2H_2O$ due to greater planarity.

The impact of structural differences between the compounds becomes obvious when comparing the optoelectronic properties. The physical color of each compound is often a good indicator towards the extent of inorganic connectivity (Figure 6): Typically, greater inorganic connectivity will result in smaller band gaps and thus darker colored solids, such as those seen in Ruddlesden-Popper type hybrid halides.[41] This is indeed what we observe for the compounds $(phenH_2)BiI_5•H_2O$ and $(2,2\text{-}bpyH_2)BiI_5$: the former, which has the chains of corner-sharing octahedra, is a dark red color while the latter, which only has $[Bi_2I_9]$ dimers, is a bright orange color. On the other hand, $(BrbpyH)BiI_4•H_2O$ has extended face-sharing octahedra yet has a similar color to that of $(2,2\text{-}bpyH_2)BiI_5$, contrary to what one would expect with extended inorganic connectivity. Diffuse reflectance reveals similar optical band gaps for these compounds (~2.07 eV), while (phenH2)BiI5•H2O has a smaller gap of ~1.85 eV (Figure 6). We believe that the gap of the $(BrbpyH)BiI_4•H_2O$ is wider than expected from this trend for three reasons: First, the face-sharing chains do not provide much dispersion and have flat bands (Figure 10), similar to that seen in the compound $(C_7H_7)BiI_4$.[16] The second is that the $(BrbpyH)^+$ cation is only singly protonated, which could influence the electronic states of the organic cation relative to $(2,2\text{-}bpyH_2)^{2+}$. Lastly, the shortest inter-inorganic chain distance of 4.6421(11) Å is too long to provide significant inter-chain orbital overlap and much larger than the largest interchain distance in $(phenH_2)BiI_5•H_2O$ (4.0314(10) Å), which would further decrease dispersion of the iodine bands.

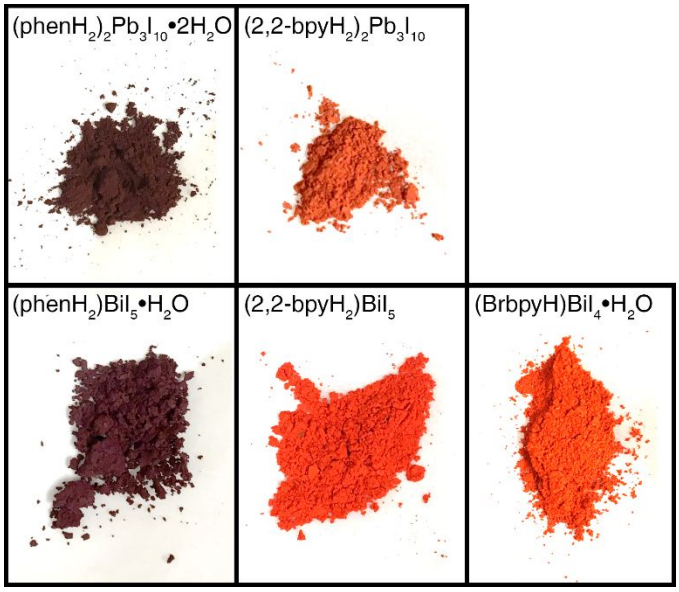

Figure 7. Brightfield images of the reported compounds in powder form.

The optical properties of the compounds $(phenH_2)_2Pb_3I_{10}•2H_2O$ and $(2,2\text{-}bpyH_2)_2Pb_3I_{10}$ follow similar trends to the Bi^{3+} compounds with $(2,2\text{-}bpyH_2)_2Pb_3I_{10}$ having a wider gap than $(phenH_2)_2Pb_3I_{10}•2H_2O$. As each of these compounds have similar inorganic connectivity (i.e., 1-dimensional chains), one would not expect much change in band gap. Nevertheless, we do observe significant changes in physical color corresponding to band gaps of ~1.77 and ~1.85 for $(phenH_2)_2Pb_3I_{10}•2H_2O$ and $(2,2\text{-}bpyH_2)_2Pb_3I_{10}$, respectively. The change in gap correlates with the inter-chain distances for these compounds, with the shortest interchain distances.

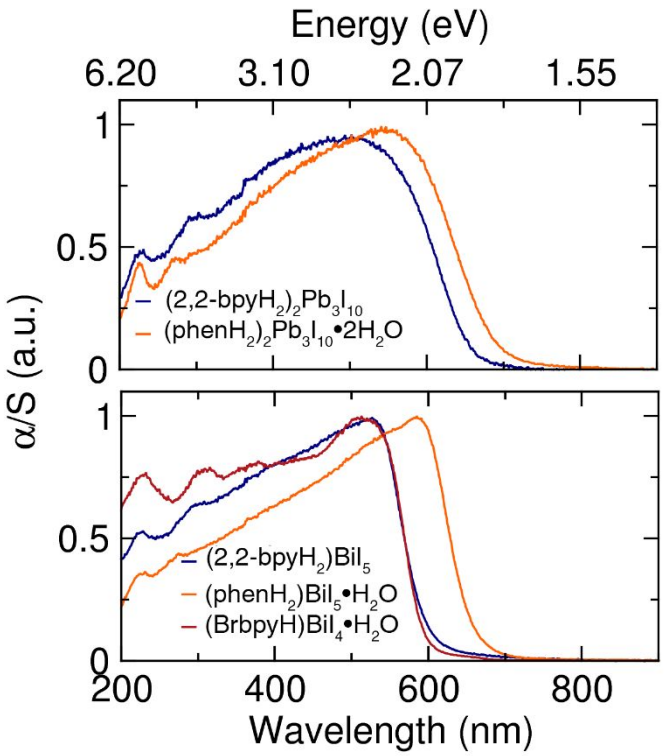

Figure 8. Top: Diffuse Reflectance of powdered $(2,2\text{-bpyH}_2)_2Pb_3I_{10}$ and $(phenH_2)_2Pb_3I_{10}\bullet 2H_2O$. Bottom: Diffuse Reflectance of powdered $(2,2\text{-bpyH}_2)BiI_5$ and $(phenH_2)BiI_5\bullet H_2O$, and $(BrbpyH)BiI_4\bullet H_2O$.

These compounds exhibit characteristics of charge-transfer semiconductors, as the valence band for each is composed of iodine p-orbitals, and the conduction band carbon and nitrogen π^* orbitals. This is similar to that observed in $(C_7H_7)MX_4$ ($M = Bi^{3+}$, Sb^{3+}; X = Cl–, Br–, I–).[16] Electronic structure calculations reveal significantly more dispersion in $(phenH_2)BiI_5\bullet H_2O$ than $(2,2\text{-bpyH}_2)BiI_5$, which arises from the extended octahedral inorganic unit in the former (Figure 10). This is the case for both the valence and conduction bands, indicating that the phen molecule provides greater dispersion, most likely due to the better overlap of neighboring molecules than 2,2-bpy. $(BrbpyH)BiI_4\bullet H_2O$ has relatively flat bands, although has a higher calculated band gap compared to $(2,2\text{-bpyH}_2)BiI_5$ even though the optical absorbance for each are very similar. This discrepancy between calculation and experimental measurement could be due to the fact that the $BrbpyBiI_4\bullet H_2O$ structure used was a supercell generated by removing every other hydrogen (due to the 50% occupancy of the H on each nitrogen of the pyridine rings). This difference could potentially change the gap as the actual positions of the hydrogen atoms maybe completely random, which could influence the charge distribution on the cations throughout the structure.

The increase of conduction band dispersion when comparing the cations is even more drastic for $(phenH_2)_2Pb_3I_{10}\bullet 2H_2O$ and $(2,2\text{-bpyH}_2)_2Pb_3I_{10}$ as shown in Figure S1. Interestingly, although the connectivity of the inorganic units are relatively similar (1-D chains), there exists greater dispersion in the

valence band of $(phenH_2)_2Pb_3I_{10}•2H_2O$. This could potentially be due to shorter interchain distances (which could enhance the dispersion) as they are shorter for $(phenH_2)_2Pb_3I_{10}•2H_2O$ (4.5936(9) Å) compared to $(2,2\text{-}bpyH_2)_2Pb_3I_{10}$ (4.6614(9) Å).

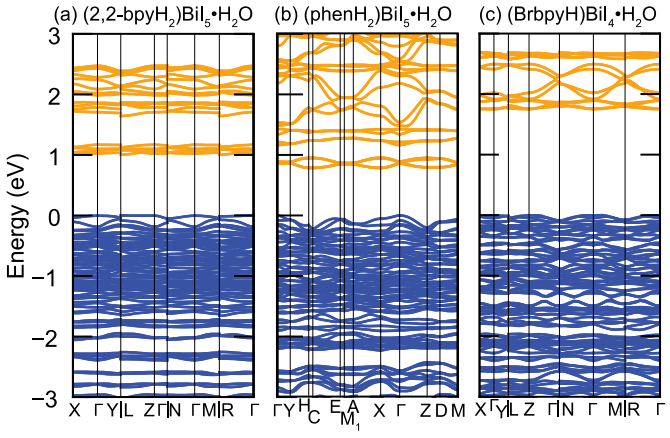

Figure 9. Band structure calculations of the compounds $(2,2\text{-}bpyH_2)BiI_5•H_2O$, $(phenH_2)BiI_5•H_2O$, and $(BrbpyH)BiI_4•H_2O$, showing the relatively flat bands from the low-dimensional crystal structures.

Taken together, these results suggest that when targeting compounds with smaller band gaps, smaller, planar cations should be used, as they will allow for efficient packing of the organic molecules while minimizing inter-chain distances of the inorganic units. Planarity can be achieved by two ways: using cations that prevent torsional twisting thus preserving planarity or incorporating atoms on the organic cation that can induce non-covalent interactions with the inorganic substructural unit. Conversely, if one is targeting compounds with wider gaps, the use of non-planar or sterically encumbered cations should be used as they can prevent extended connectivity of the inorganic unit, while also spatially separating them from one another to eliminate any inter-chain interactions.

Conclusions.

Six new organic metal-halide compounds have been synthesized and characterized to probe how planarity of aromatic cations affects the structure and optoelectronic properties. The dications 2,2'-bipyridine-1,1'-diium and 1,10-phenanthroline-1,10-diium were used to compare how the planarity of the latter changes the structure in relation the former. We find that it has a strong effect on the structures of the synthesized compounds, $(phenH_2)_2Pb_3I_{10}•2H_2O$, $(2,2\text{-}bpyH_2)_2Pb_3I_{10}$, $(phenH_2)BiI_5•H_2O$ and $(2,2\text{-}bpyH_2)BiI_5$. The ability to twist around the C–C bond in 2,2-bpy leads to a *trans* configuration in both $(2,2\text{-}bpyH_2)_2Pb_3I_{10}$ and $(2,2\text{-}bpyH_2)BiI_5$, whereas $(phenH_2)_2Pb_3I_{10}•2H_2O$ and $(phenH_2)BiI_5•H_2O$ require a *cis* configuration due to the C-C backbone resulting in retention of planarity and more efficient stacking

compare to the former compounds. We find that this more efficient packing leads to smaller optical band gaps, which electronic structure calculations revealed to be due to greater dispersion in the valence and conduction bands. We then investigated how halogenation of 2,2'-bipyridine affects the structure and properties by synthesizing the new compound, (BrbpyH)BiI_4•H_2O, which contains the cation 6,6'-dibromo-2,2'-bipyridine-1,1'-diium. We find that the bromine atoms induce a *cis* configuration in the cations driven by the propensity to form non-covalent interactions between the bromine and iodine atoms of the inorganic unit. This leads to efficient packing with planarity of the cation, however both have wider band gaps due to significantly increased interatomic distances between inorganic substructural units. These results show that both planarity, steric effects, and non-covalent interactions between the inorganic and organic substructural units can be used as a means of directing structure in hybrid metal-halide compounds, which can directly impact the functionality of a given material.

Acknowledgements

This work was supported by grant DE-SC0016083 funded by the U.S. Department of Energy, Office of Science. JRN acknowledges additional support from Research Corporation for Science Advancement through a Cottrell Scholar Award and the A.P. Sloan Foundation for assistance provided from a Sloan Research Fellowship.

Supporting Information

The supporting information includes Powder X-ray diffraction, band structure calculations for (2,2-bpyH_2)$_2$$Pb_3I_{10}$, (phen$H_2$)$_2$$Pb_3I_{10}$•$2H_2O$, and atomic positions derived from single crystal X-ray diffraction. Also included are supplementary crystal information files (cif) of new structures. The single crystal results are available in The Cambridge Crystallographic Data Center: phenBiI_5•H_2O: 1945574; (2,2-bpyH_2)BiI_5: 1945579; BrbpyBiI_4•H_2O: 1945575; (2,2-bpyH_2)$_2$$Pb_3I_{10}$: 1945576; phen$_2$$Pb_3I_{10}$•$2H_2O$: 1945577.

References.

1. Snaith, H. J., Perovskites: The Emergence of a New Era for Low-Cost, High-Efficiency Solar Cells. *J. Phys. Chem. Lett.* **2013,** *4*, 3623-3630.
2. Manser, J. S.; Christians, J. A.; Kamat, P. V., Intriguing Optoelectronic Properties of Metal Halide Perovskites. *Chem. Rev.* **2016,** *116*, 12956-13008.
3. Smith, M. D.; Crace, E. J.; Jaffe, A.; Karunadasa, H. I., The Diversity of Layered Halide Perovskites. *Annu. Rev. Mater. Res.* **2018,** *48*, 111-136.
4. Li, W.; Wang, Z.; Deschler, F.; Gao, S.; Friend, R. H.; Cheetham, A. K., Chemically Diverse and Multifunctional Hybrid Organic–Inorganic Perovskites. *Nat. Rev. Mater.* **2017,** *2*, 16099.
5. Stoumpos, C. C.; Malliakas, C. D.; Kanatzidis, M. G., Semiconducting Tin and Lead Iodide Perovskites with Organic Cations: Phase Transitions, High Mobilities, and Near-Infrared Photoluminescent Properties. *Inorg. Chem.* **2013,** *52*, 9019-9038.
6. Mitzi, D. B.; Feild, C. A.; Harrison, W. T. A.; Guloy, A. M., Conducting Tin Halides With a Layered Organic-Based Perovskite Structure. *Nature* **1994,** *369*, 467-469.

7. Chen, Y.; Sun, Y.; Peng, J.; Tang, J.; Zheng, K.; Liang, Z., 2D Ruddlesden–Popper Perovskites for Optoelectronics. *Adv. Mater.* **2017,** *30*, 1703487.
8. Slavney, A. H.; Hu, T.; Lindenberg, A. M.; Karunadasa, H. I., A Bismuth-Halide Double Perovskite with Long Carrier Recombination Lifetime for Photovoltaic Applications. *J. Am. Chem. Soc.* **2016,** *138*, 2138-2141.
9. Pazoki, M.; Johansson, M. B.; Zhu, H.; Broqvist, P.; Edvinsson, T.; Boschloo, G.; Johansson, E. M. J., Bismuth Iodide Perovskite Materials for Solar Cell Applications: Electronic Structure, Optical Transitions, and Directional Charge Transport. *J. Phys. Chem. C* **2016,** *120*, 29039-29046.
10. Mitzi, D. B., Templating and Structural Engineering in Organic–Inorganic Perovskites. *J. Chem. Soc., Dalton Trans.* **2001**, 1-12.
11. Eperon, G. E.; Stranks, S. D.; Menelaou, C.; Johnston, M. B.; Herz, L. M.; Snaith, H. J., Formamidinium Lead Trihalide: a Broadly Tunable Perovskite for Efficient Planar Heterojunction Solar Cells. *Energy Environ. Sci.* **2014,** *7*, 982-988.
12. Smith, I. C.; Hoke, E. T.; Solis-Ibarra, D.; McGehee, M. D.; Karunadasa, H. I., A Layered Hybrid Perovskite Solar-Cell Absorber with Enhanced Moisture Stability. *Angew. Chem.* **2014,** *126*, 11414-11417.
13. Evans, H. A.; Labram, J. G.; Smock, S. R.; Wu, G.; Chabinyc, M. L.; Seshadri, R.; Wudl, F., Mono- and Mixed-Valence Tetrathiafulvalene Semiconductors (TTF)BiI_4 and $(TTF)_4BiI_6$ with 1D and 0D Bismuth-Iodide Networks. *Inorg. Chem.* **2017,** *56*, 395-401.
14. Zhang, W.; Tao, K.; Ji, C.; Sun, Z.; Han, S.; Zhang, J.; Wu, Z.; Luo, J., $(C_6H_{13}N)_2BiI_5$: A One-Dimensional Lead-Free Perovskite-Derivative Photoconductive Light Absorber. *Inorg. Chem.* **2018,** *57*, 4239-4243.
15. Park, B.-W.; Philippe, B.; Zhang, X.; Rensmo, H.; Boschloo, G.; Johansson, E. M. J., Bismuth Based Hybrid Perovskites $A_3Bi_2I_9$ (A: Methylammonium or Cesium) for Solar Cell Application. *Adv. Mater.* **2015,** *27*, 6806-6813.
16. Oswald, I. W. H.; Mozur, E. M.; Moseley, I. P.; Ahn, H.; Neilson, J. R., Hybrid Charge-Transfer Semiconductors: $(C_7H_7)SbI_4$, $(C_7H_7)BiI_4$, and Their Halide Congeners. *Inorg. Chem.* **2019**.
17. Maughan, A. E.; Kurzman, J. A.; Neilson, J. R., Hybrid Inorganic–Organic Materials with an Optoelectronically Active Aromatic Cation: $(C_7H_7)_2SnI_6$ and $C_7H_7PbI_3$. *Inorg. Chem.* **2015,** *54*, 370-378.
18. Savory, C. N.; Palgrave, R. G.; Bronstein, H.; Scanlon, D. O., Spatial Electron-hole Separation in a One Dimensional Hybrid Organic–Inorganic Lead Iodide. *Sci. Rep.* **2016,** *6*, 20626.
19. Hu, J.; Oswald, I. W. H.; Hu, H.; Stuard, S. J.; Nahid, M. M.; Yan, L.; Chen, Z.; Ade, H.; Neilson, J. R.; You, W., Aryl-Perfluoroaryl Interaction in Two-Dimensional Organic–Inorganic Hybrid Perovskites Boosts Stability and Photovoltaic Efficiency. *ACS Materials Letters* **2019**, 171-176.
20. Hu, J.; Oswald, I. W. H.; Stuard, S. J.; Nahid, M. M.; Zhou, N.; Williams, O. F.; Guo, Z.; Yan, L.; Hu, H.; Chen, Z.; Xiao, X.; Lin, Y.; Yang, Z.; Huang, J.; Moran, A. M.; Ade, H.; Neilson, J. R.; You, W., Synthetic Control Over Orientational Degeneracy of Spacer Cations Enhances Solar Cell Efficiency in Two-Dimensional Perovskites. *Nat. Comm.* **2019,** *10*, 1276.
21. Slavney, A. H.; Smaha, R. W.; Smith, I. C.; Jaffe, A.; Umeyama, D.; Karunadasa, H. I., Chemical Approaches to Addressing the Instability and Toxicity of Lead–Halide Perovskite Absorbers. *Inorg. Chem.* **2017,** *56*, 46-55.
22. Lemmerer, A.; Billing, D. G., Effect of Heteroatoms in the Inorganic–Organic Layered Perovskite-Type Hybrids $[(ZC_nH_{2n}NH_3)_2PbI_4]$, n = 2, 3, 4, 5, 6; Z = OH, Br and I; and $[(H_3NC_2H_4S_2C_2H_4NH_3)PbI_4]$. *CrystEngComm* **2010,** *12*, 1290-1301.
23. Solis-Ibarra, D.; Karunadasa, H. I., Reversible and Irreversible Chemisorption in Nonporous-Crystalline Hybrids. *Angew. Chem. Int. Ed.* **2014,** *53*, 1039-1042.
24. Smith, M. D.; Pedesseau, L.; Kepenekian, M.; Smith, I. C.; Katan, C.; Even, J.; Karunadasa, H. I., Decreasing the Electronic Confinement in Layered Perovskites Through Intercalation. *Chem. Sci.* **2017,** *8*, 1960-1968.
25. Solis-Ibarra, D.; Smith, I. C.; Karunadasa, H. I., Post-Synthetic Halide Conversion and Selective Halogen Capture in Hybrid Perovskites. *Chem. Sci.* **2015,** *6*, 4054-4059.
26. Krause, L.; Herbst-Irmer, R.; Sheldrick, G. M.; Stalke, D., Comparison of Silver and Molybdenum Microfocus X-ray Sources for Single-Crystal Structure Determination. *J. Appl. Crystallogr.* **2015,** *48*, 3-10.
27. Sheldrick, G., SHELXT - Integrated Space-Group and Crystal-Structure Determination. *Acta Crystallogr. A* **2015,** *71*, 3-8.
28. Sheldrick, G., A Short History of SHELX. *Acta Crystallogr. A* **2008,** *64*, 112-122.
29. Spek, A., Single-Crystal Structure Validation With the Program PLATON. *J. Appl. Crystallogr.* **2003,** *36*, 7-13.
30. Kresse, G.; Furthmüller, J., Efficient Iterative Schemes for Ab Initio Total-Energy Calculations Using a Plane-Wave Basis Set. *Phys. Rev. B* **1996,** *54*, 11169-11186.
31. Hafner, G. K. a. J., Norm-Conserving and Ultrasoft Pseudopotentials for First-row and Transition Elements. *J. Phys.: Condens. Matter* **1994,** *6*, 8245–8257.
32. Perdew, J. P.; Burke, K.; Ernzerhof, M., Generalized Gradient Approximation Made Simple. *Phys. Rev. Lett.* **1996,** *77*, 3865-3868.

33. Perdew, J. P.; Ruzsinszky, A.; Csonka, G. I.; Vydrov, O. A.; Scuseria, G. E.; Constantin, L. A.; Zhou, X.; Burke, K., Restoring the Density-Gradient Expansion for Exchange in Solids and Surfaces. *Phys. Rev. Lett.* **2008,** *100*, 136406.
34. Setyawan, W.; Curtarolo, S., High-Throughput Electronic Band Structure Calculations: Challenges and Tools. *Comput. Mater. Sci* **2010,** *49*, 299-312.
35. Ganose, A. M. J., Adam J.; Scanlon, David O., Sumo: Command-Line Tools for Plotting and Analysis of Periodic Ab Initio Calculations *J. Open Source Softw.* **2018,** *3*, 717.
36. Momma, K.; Izumi, F., VESTA 3 for Three-Dimensional Visualization of Crystal, Volumetric and Morphology Data. *J. Appl. Crystallogr.* **2011,** *44*, 1272-1276.
37. Lemmerer, A.; Billing, D. G., Lead Halide Inorganic–Organic Hybrids Incorporating Diammonium Cations. *CrystEngComm* **2012,** *14*, 1954-1966.
38. Göller, A.; Grummt, U.-W., Torsional Barriers in Biphenyl, 2,2′-Bipyridine and 2-Phenylpyridine. *Chem. Phys. Lett.* **2000,** *321*, 399-405.
39. Merritt, L. L.; Schroeder, E., The Crystal Structure of 2,2'-Bipyridine. *Acta Crystallogr.* **1956,** *9*, 801-804.
40. Oswald, I. W. H.; Koegel, A. A.; Neilson, J. R., General Synthesis Principles for Ruddlesden–Popper Hybrid Perovskite Halides from a Dynamic Equilibrium. *Chem. Mater.* **2018,** *30*, 8606-8614.
41. Stoumpos, C. C.; Cao, D. H.; Clark, D. J.; Young, J.; Rondinelli, J. M.; Jang, J. I.; Hupp, J. T.; Kanatzidis, M. G., Ruddlesden–Popper Hybrid Lead Iodide Perovskite 2D Homologous Semiconductors. *Chem. Mater.* **2016,** *28*, 2852-2867.

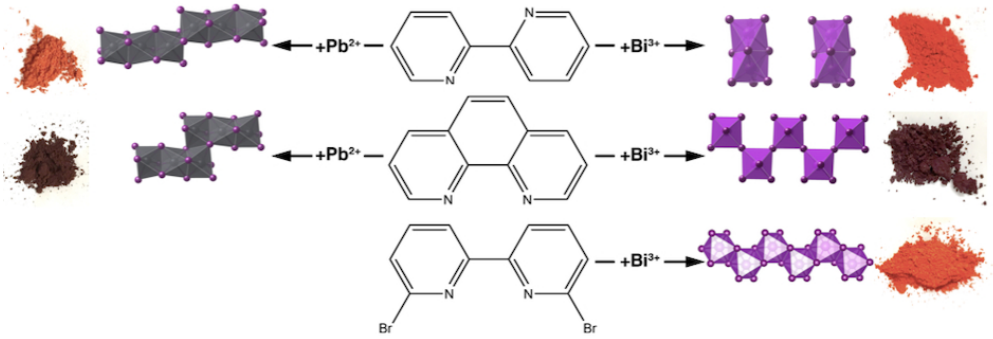
+Pb2+
+Bi3+
+Pb2+
+Bi3+
+Bi3+
N
N
N
N
N
N
Br
Br

The structure and planarity of aromatic organic cations directly influence both the inorganic connectivity and the resulting optical properties in hybrid semiconductors, thus providing tunability for optoelectronic applications.